Tradeoff between cost and accuracy in large-scale surface water dynamic modeling

Augusto Getirana[1,2], Christa Peters-Lidard[1], Matthew Rodell[1], Paul D. Bates[3]

1 Hydrological Sciences Laboratory, NASA Goddard Space Flight Center, Greenbelt, MD

2 Earth System Science Interdisciplinary Center, University of Maryland, College Park, MD

3 School of Geographical Sciences, University of Bristol, Bristol, UK

Correspondence to: A. Getirana (augusto.getirana@nasa.gov)

Abstract

Recent efforts have led to the development of the local inertia formulation (INER) for an accurate but still cost-efficient representation of surface water dynamics, compared to the widely used kinematic wave equation (KINE). In this study, both formulations are evaluated over the Amazon basin in terms of computational costs and accuracy in simulating streamflows and water levels through synthetic experiments and comparisons against ground-based observations. Varying time steps are considered as part of the evaluation and INER at 60-second time step is adopted as the reference for synthetic experiments. Five hybrid (HYBR) realizations are performed based on maps representing the spatial distribution of the two formulations that physically represent river reach flow dynamics within the domain. Maps have fractions of KINE varying from 35.6% to 82.8%. KINE runs show clear deterioration along the Amazon river and main tributaries, with maximum RMSE values for streamflow and water level reaching

7827$m^3.s^{-1}$ and 1379cm near the basin's outlet. However, KINE is at least 25% more efficient than INER with low model sensitivity to longer time steps. A significant improvement is achieved with HYBR, resulting in maximum RMSE values of 3.9-292$m^3.s^{-1}$ for streamflows and 1.1-28.5cm for water levels, and cost reduction of 6-16%, depending on the map used. Optimal results using HYBR are obtained when the local inertia formulation is used in about one third of the Amazon basin, reducing computational costs in simulations while preserving accuracy. However, that threshold may vary when applied to different regions, according to their hydrodynamics and geomorphological characteristics.

1. Introduction

Being able to accurately simulate surface water dynamics is essential for understanding their impacts on regional and global climate and nutrient cycles, determining present and future water availability for human activities and minimizing impacts of extreme events. For these reasons, numerous efforts have led to the development of models and formulations capable of simulating rivers and floodplains at different scales. The *Saint-Venant* equations, which represent the one-dimensional gradually varied unsteady flow in open channels through simplifications applied to the *Navier-Stokes* equations, provide the most complete 1-D description of river hydrodynamics. They are based on the mass and the momentum conservation laws, respectively, as follows (Cunge et al., 1980):

$$\frac{\partial Q}{\partial x} + \frac{\partial A}{\partial t} = 0 \qquad (1)$$

$$\frac{\partial}{\partial x}\left[\frac{Q^2}{A}\right] + \frac{\partial Q}{\partial t} + gA\frac{\partial h}{\partial x} = gAi_o - gAi_f \qquad (2)$$

(i) (ii) (iii) (iv) (v)

where Q [$m^3.s^{-1}$] is streamflow, t [s] is time, x [m] is river longitudinal space coordinate, h [m] is river water depth, g [$m.s^{-2}$] is acceleration due to gravity, A [m^2] is the cross sectional flow area perpendicular to the flow direction and i_0 [$m.m^{-1}$] and i_f [$m.m^{-1}$] are the bed slope and friction slope in the x-direction. The momentum conservation law [Eq. (2)] is composed of the balance of (i) convective and (ii) local inertia with (iii) pressure, (iv) gravity and (v) friction forces.

Whilst studies have demonstrated the feasibility of implementing the full Saint-Venant equations at regional scales (e.g. Paz et al., 2011; Paiva et al., 2013), the non-negligible increase of computational costs and input data constraints are still limiting factors for their implementation globally. In order to avoid these limitations, continental and global scale river routing schemes have been developed based on simplified relationships between water volume storage within a river reach and its outflow (Vorosmarty et al., 1989; Lohmann et al., 1996; Oki et al., 1998; Arora et al., 1999), the Muskingum method and variations (Collischonn et al., 2007; David et al., 2011; Getirana et al., 2014a), the kinematic wave (KINE: Decharme et al., 2011; Getirana et al., 2012; Li et al., 2015) and diffusive wave (DIFF: Yamazaki et al., 2011; Luo et al., 2017) methods. Such models have been useful in land surface model (LSM) evaluation (e.g. Getirana et al., 2014a,b,c, 2015, 2017), anthropogenic impacts on the water cycle (Haddeland et al., 2006; Hanasaki et al., 2006; Döll et al., 2009; Biemans et al., 2011), data assimilation experiments (e.g. Kumar et al., 2015, 2016), and global water budget accounting (Clark et al., 2015), amongst other applications. Most of existing global scale river routing schemes, in particular those coupled with general circulation models, still use KINE or more basic formulations (e.g. Miller et al., 1994; Decharme et al., 2011), insuring a low computational cost while providing spatial and temporal freshwater discharges from continents into the oceans accurate enough for climate modeling purposes.

64 More recently, Bates et al. (2010) and de Almeida et al. (2012) suggested a new explicit solution
65 for the *Saint-Venant* momentum equation only neglecting the convective term (i). Compared to
66 DIFF, it includes the local inertia term (ii), improving numerical stability and allowing
67 simulations with longer time steps. The local inertia formulation (INER) has been implemented
68 in the Catchment-Based Macro-scale Floodplain (CaMa-Flood: Yamazaki et al., 2011) river
69 routing scheme and evaluated globally (Yamazaki et al., 2013). Yamazaki *et al.* compared the
70 new formulation against DIFF in terms of numerical stability, and streamflow and water level
71 simulations at selected gauges. Conclusions were that INER was capable of running global
72 experiments at longer time steps while keeping numerical stability. The authors discuss how
73 computational costs can be improved in further large-scale applications, but no quantitative
74 information is provided.

75 Although synthetic and small-scale experiments are the most common way to quantitatively
76 compare flood modeling techniques (e.g. Bates & De Roo, 2000; Bates et al., 2010),
77 comprehensive tradeoff evaluations in terms of cost and accuracy at the large scale are not
78 commonly found in the literature. Additionally, to date, no detailed comparison between INER
79 and KINE has been undertaken, and this therefore is the objective of this paper. Both
80 formulations have been implemented in the Hydrological Modeling and Analysis Platform
81 (HyMAP: Getirana et al., 2012) and are evaluated here using synthetic experiments and
82 comparisons against observations over the Amazon basin. Experiments are designed with
83 varying time steps, and efficiency is evaluated in terms of computational costs and accuracy in
84 simulating streamflows and water levels.

Moussa and Bocquillon (1996) initially proposed a method that analyzes flows using Saint-Venant equations as the superposition of a permanent regime and a perturbation of the steady uniform flow. Getirana and Paiva (2013) adapted the technique to map flood wave types at the large scale and evaluated it over the Amazon. They also highlighted the importance of using such maps in the development of models combining multiple formulations in order to minimize computational costs, but preserving accuracy. Indeed, combining methods with different levels of complexity has been a common practice in flood modeling to optimize computational costs. For example, Paiva et al. (2013) coupled the Muskingum-Cunge method (Cunge et al., 1980) and the full Saint-Venant equations in order to simulate the upper Amazon basin. Following that direction, a hybrid model (HYBR), combining both the kinematic wave equation and local inertia formulation, is also implemented in HyMAP and evaluated in this study. Although we acknowledge the existence of numerous flood modeling techniques, such as those listed earlier in the text, and also analytical solutions of the kinematic wave equation (e.g. Reggiani et al., 2014), we limited this comparison to the numerical solutions of KINE, INER and HYBR. This decision is based on the consideration that the kinematic wave and the local inertia formulation are both physically-based and represent extremes of the simplification spectrum of the full Saint-Venant equations.

2. The HyMAP global-scale river routing scheme

HyMAP is a global-scale river routing scheme composed of the following modules: (1) surface runoff and baseflow time delays; (2) river-floodplain interface; (3) flow in both river channels and floodplains; and (4) evaporation from floodplains.

106 The temporal change of water storage in rivers and floodplains of a grid cell, *S*, is defined by the
107 continuity equation [Eq. (3)] considering LSM-based total runoff (after passing through time
108 delay reservoirs), *Qc*, river and floodplain discharges to the downstream grid point, Q^r and Q^f,
109 and from the upstream grid points, Qup^r and Qup^f, and evaporation from open waters (i.e.
110 rivers and floodplains), *E*:

111 $$S_{t+dt} = S_t + \left[Qc_t + \sum_{k=1}^{nUp}\left(Qup_t^{r,k} + Qup_t^{f,k}\right) - Q_t^r - Q_t^f - E_t^{r,f}\right]dt \quad (3)$$

112 where subscripts *r* and *f* represent river channel and floodplain variables, respectively. *dt* stands
113 for time step and the index *k* the *nUp* upstream grid cells of the target grid point.

114 Time delays are represented in HyMAP at the sub-grid-scale where, in each grid cell, both
115 surface runoff and baseflow derived from LSMs pass through individual linear reservoirs with
116 appropriate time-delay factors. The current HyMAP parameterization for the Amazon basin
117 considers the baseflow time delay as 45 days. The surface runoff time delay T_s is computed for
118 each grid cell following the Kirpich's (1940) formula:

119 $$T_s = 3600\left(0.868\frac{\Delta x^3}{\Delta h}\right)^{0.385} \quad (4)$$

120 where Δx [km] is the distance between the farthest point within a grid cell and its outlet, and Δh
121 [m] is the difference between the maximum and minimum elevations of the pathway. This
122 formula was initially developed for small agricultural areas, but has been satisfactorily applied to
123 larger regions (e.g. Collischonn et al., 2007; Getirana et al., 2014a). Both linear reservoir outputs
124 total the discharge produced in each grid cell, *Qc* [$m^3.dt^{-1}$], flowing to the river network.

Water overflows to floodplains when the river channel water height h_r [m] is higher than the bank height, H. This process is considered instantaneous at each time step. This means that water surface elevations of the river channel and the floodplain are the same. Elevation profiles are used to represent floodplains. As a result, floodplain water extent and storage can be derived from the floodplain water elevation, h_f.

The river and floodplain water exchange at each time step is represented as follows:

$$if\ S_{t+dt} \le S^{rmax}: \begin{matrix} S^r_{t+dt} = S \\ h^r_{t+dt} = S^r_{t+dt}/(W \cdot L) \\ S^f_{t+dt} = 0 \\ h^f_{t+dt} = 0 \end{matrix} \quad (5)$$

$$else: \begin{matrix} S^r_{t+dt} = S_{t+dt} - S^f_{t+dt} \\ h^r_{t+dt} = S^r_{t+dt}/(W \cdot L) \\ S^f_{t+dt} = \int_0^{A^f_{t+1}} \left[h^f_{t+dt} - h\left(A^f_{t+dt}\right)\right] dA \\ h^f_{t+dt} = h^r_{t+dt} - H \end{matrix} \quad (6)$$

where S [m^3] stands for the total water storage in the grid cell, S_r [m^3] and S_f [m^3] the river channel and floodplain water storages, h_r [m] and h_f [m] river water depths, W [m] the river width, L [m] the river length and A_f [m^2] the flooded area. $S_{r\,\max}$ [m^3] stands for the river bankfull water storage, and is given as $S_{r\max}=H\times W\times L$, where H [m] is the river bankfull height.

Using the kinematic wave equation, considering a rectangular river cross section and large width-to-depth ratio, water discharge through a grid cell river reach at time step t+dt, Q_{t+dt} [$m^3 \cdot s^{-1}$], can be defined as

$$Q_{t+dt} = \frac{1}{n} \cdot i_0^{1/2} \cdot W \cdot h_t^{5/3} \quad (7)$$

where n is the Manning roughness coefficient. i_0 is derived from topographic information and corresponds to the slope between the target and downstream grid cells. A minimum i_0 threshold of 10^{-5}m.m^{-1} is used in order to avoid negative or very small topography slope caused by DEM errors.

Following the explicit solution presented in Bates et al. (2010) and improved in Almeida et al. (2012), the local inertia formulation, for the same river cross sections defined above, can be defined as

$$Q_{t+dt} = \frac{Q_t + g \cdot h_t \cdot dt \cdot i_f}{\left(1 + g \cdot dt \cdot n^2 |\cdot Q_t| / h_t^{10/3}\right)} \quad (8)$$

For HyMAP to be run in hybrid mode, a map determining the spatial distribution of flow types has to be provided.

In HyMAP, rivers and floodplains flow independently from a grid cell to another, and have their hydrodynamics calculated separately using their own channel characteristics, but the same equations. At each time step, the average floodplain width, depth and bed height are defined as

$$\overline{W}_f = \frac{A_f}{L} \quad (9)$$

$$\overline{h}_f = \frac{S_f}{A_f} \quad (10)$$

$$\bar{z}_f = z_r + h_r - \overline{h}_f \quad (11)$$

For the kinematic wave equation, i_0 is considered the same for both rivers and floodplains. River width W and bankfull height H are both defined based on empirical relationships with long-term average discharges, and the Manning coefficient of river channels n_r [-] varies as a function of H.

The Manning coefficient for floodplains, n_f [-], is spatially distributed as a function of vegetation types derived from a static map (Masson et al. 2003), where larger values correspond to dense vegetated areas and lower values to sparser vegetated regions. More details on HyMAP parameterization are found in Getirana et al. (2012; 2013).

2.1. Optimal time step for numerical stability

The Courant–Freidrichs–Levy (CFL) condition is used in order to determine the optimal time step for numerical stability for INER:

$$C_r = \frac{V \partial t}{\partial x} \qquad (12)$$

where C_r stands for the non-dimensional Courant number and V is a characteristic velocity [m.s^{-1}]. Numerical stability is obtained when C_r is less than 1. V can be defined for the local inertial form of the shallow water equations as (Bates et al., 2010):

$$V = \sqrt{gh} \qquad (13)$$

Eq. (12) can be rewritten as follows, defining the maximum time step needed to keep numerical stability:

$$dt_{max} = \alpha \frac{dx}{\sqrt{g h_t}} \qquad (14)$$

where α is a coefficient that is used to ensure that the selected time step remains at all times smaller than the maximum threshold for stability. Eq. (14) has been implemented in HyMAP to determine optimal time intervals and α was set as 0.9 for all experimental runs (i.e. the actual time step used is 90% of the theoretical maximum).

3. Experimental design

Experiments are designed with the following objectives: (i) to quantify the gains of using the more complex INER formulation over the simplified KINE, in terms of accuracy in simulating water levels and streamflows; (ii) to evaluate the sensitivity of both formulations to model time steps; and (iii) to determine the added value in considering a hybrid model HYBR that combines both formulations.

The evaluation is performed in terms of accuracy and computational costs and is composed of two stages: (1) synthetic experiments and (2) evaluation against observations. In stage 1, model accuracy is quantified using the root mean square error (RMSE) against a control simulation. Computational costs are determined in terms of time needed to run the model (excluding initialization and input/output processing). Synthetic experiments are based on the Amazon basin and performed for two years (1999-2000), after a 1-year spin up. The same initial condition is used in all experiments. The INER experiment at 60s time step is considered as the control simulation for synthetic experiments, as will theoretically be the highest quality simulation, and the evaluation is performed in terms of streamflows and river water depths/water elevations. In order to evaluate the sensitivity to time steps, five realizations are performed for INER and KINE, and the following intervals considered: 60s, 120s, 300s, 600s and 1200s. For consistency, intervals are fixed for each run. This means that dt_{max} is computed for each run with Eq. (14), but not used to constrain time steps.

Although ocean tides play an important role in river dynamics near the outlet, they have been neglected in this study. Thus, the downstream boundary water elevation at the Amazon River mouths is set to zero meters constant over time.

In stage 2, the evaluation against observations has been performed for the 2002-2008 period using daily ground-based streamflow observations at 144 gauges and satellite-based water elevations at 396 locations (see Fig. 1 for locations). Runs have been performed at a 15-minute time step. Streamflow gauges are operated by the Brazilian Water Agency (*Agencia Nacional de Aguas* – ANA) and the water elevation dataset was derived from the Envisat satellite and is available on the Hydroweb website (Cretaux et al., 2011). Envisat operated from 2002 to 2010 at a 35-day cycle and absolute water elevation errors within the Amazon basin are on the order of tens of centimeters (Da Silva et al., 2011).

Daily streamflow is evaluated using the Nash-Sutcliffe (NS) coefficient:

$$NS = 1 - \frac{\sum_{t=1}^{nt}(y_t - x_t)^2}{\sum_{t=1}^{nt}(y_t - \bar{y}_t)^2} \qquad (15)$$

where t is the time step, and nt represents the total number of days with observed data. The variables x and y are, respectively, the simulated and observed signals at time step t, while y_{max}, y_{min} and $\bar{y}$ represent the respective maximum, minimum and mean values of the target signals for the entire period. *NS* ranges from -∞ to 1, where 1 is the optimal case, while zero means that simulations represent observed signals as well as the average of observations. NS of anomalies (NSA) is used to evaluate bias-corrected river water depth simulations against satellite-based water elevations (Getirana et al., 2013). Bias correction was performed as a solution to eliminate datum differences and eventual errors in the DEM, satellite observations, riverbed height estimates and river width. NSA is defined as follows:

$$NSA = 1 - \frac{\sum_{t=1}^{nt}[(y_t - \bar{y}_t) - (x_t - \bar{x}_t)]^2}{\sum_{t=1}^{nt}(y_t - \bar{y}_t)^2} \qquad (16)$$

where $\bar{x}$ stands for the mean value of the simulated signal for the entire period.

HyMAP runs over the Amazon basin at 0.25° spatial resolution and simulations were performed using a single 2.6 GHz Intel Xeon Haswell processor on the NASA Center for Climate Simulation's Discover system. Daily surface runoff and baseflow were derived from a long term run using the Noah 3.3 LSM (Ek et al., 2003) forced with the Princeton University meteorological dataset (Sheffield et al., 2006), with a rescaled precipitation matching the ORE-HYBAM (*Observatoire de Recherche en Environnement - Hydrologie du Bassin de l'Amazone*; Guimberteau et al., 2012) dataset. Details on the LSM run can be found in Getirana et al. (2014b). All model runs were executed in the NASA Land Information System (LIS: Kumar et al., 2006).

4. Results and discussion

4.1. Synthetic experiments

According to results presented in Fig. 2, KINE satisfactorily represents the hydrodynamics in most of the basin, with low RMSE values for both river water depth and streamflow simulations. However, a significant deterioration of these variables along the Amazon River and main tributaries is observed, as represented by the darker colors in the figures. This deterioration is more evident near the basin's outlet, which could be due to the incapacity of KINE to represent backwater effects. In terms of river water depths, KINE at dt=60s results in mean RMSE values of ~19cm, relative to INER at dt=60s, with a maximum value reaching ~1379cm. Average and maximum RMSE values for streamflows are ~52$m^3.s^{-1}$ and ~7827$m^3.s^{-1}$, respectively.

241 In terms of time step impacts on model accuracy, even though KINE runs result in deteriorated
242 RMSE values over main rivers, additional realizations confirm the low model sensitivity to
243 longer dt, resulting in very similar coefficient values for river water depths and streamflows. For
244 example, mean RMSE values for simulations at dt=10800s are 19.93cm and 52.97$m^3.s^{-1}$,
245 respectively. This represents nominal degradations of 3.6% and 1.3%, compared to the
246 experiment at dt=60s. Realizations performed with INER show that time steps up to 900s result
247 in gradual, but still nominal, changes in RMSE values for both variables, as shown in Fig. 3. The
248 INER realization at 1200s time step presents non-negligible deterioration, mostly occurring in
249 the lower and central Amazon and Negro Rivers, and lower Madeira River. On the other hand,
250 INER in CaMa-Flood is stable at that time step and spatial resolution (Yamazaki et al., 2013). In
251 that sense, further investigation was carried out in order to identify the reason why such a
252 limitation occurs in HyMAP. Similar simulations considering static floodplains (i.e. no flow in
253 floodplain from a grid cell to another) were performed in order to determine the sensitivity of
254 such a configuration to time step. As a result, it was verified that simulations with static
255 floodplains are stable with dt≤1800s, meaning that the deterioration observed in INER runs at
256 1200s are due to numerical instability caused by more restrictive CFL conditions in the
257 floodplain dynamics. Indeed, this empirical result matches with the CFL condition, computed for
258 the whole experimental period, which shows that the maximum stable time step for HyMAP runs
259 over the Amazon at 0.25 degrees using the local inertia formulation and floodplain dynamics is
260 1200s. It is worth noting that HyMAP and CaMa-Flood use different river network
261 parameterizations, and that difference may play a major role in computing optimal time steps.

262 Computational costs for running HyMAP for two years are linearly proportional to the number of
263 time steps used in the realizations. INER costs varied from 1017 seconds at dt=60s to 51 seconds

at a dt=1200s (see Table 1 for computational cost and accuracy summary). This is 25% longer than the corresponding realizations with KINE (812 and 41 seconds, respectively). However, since the kinematic wave shows low sensitivity to longer time steps, one could obtain similar errors with time steps as long as 10800s (or more), as shown in Table 1. This means that significantly cheaper runs (at least 15 times faster) can provide outputs with the same margin of error. At dt=900s (the longest time step for INER with demonstrated stability), the mean RMSE for bias-corrected river water depths is 0.03cm, with a maximum value of 0.5cm. For streamflows, values are $0.17 m^3.s^{-1}$ and $62.3 m^3.s^{-1}$, respectively, which are nominal compared to the absolute numbers of each variable.

Flow type maps applied to HYBR were generated based on absolute values of differential RMSE ($|\Delta rmse| = |rmse_{INER} - rmse_{KINE}|$) between KINE and INER at dt=60s. Five $|\Delta rmse|$ thresholds were considered in order to determine their spatial distribution: 1cm, 5cm, 10cm, 15cm and 20cm. These values represent a good flow type distribution spectrum for HYBR. Fig. 4 shows maps with the spatial distribution of different flow types and their respective fractions within the Amazon basin. As shown in the figure, the fraction of pixels within the basin being represented by the kinematic wave equation (f_{KINE}) exponentially increases with $|\Delta rmse|$ threshold limits. f_{KINE} covers 35.6% of the basin if the threshold is 1cm (i.e. $|\Delta rmse| \leq 1cm$ is considered as an acceptable error), mostly representing headwater grid cells. The fractions increase to 63.5% for 5cm and to 82.8% for 20cm.

The local inertia formulation is not as used over the basin when thresholds increase, except along main rivers and main tributaries. Computational costs are linearly related to f_{KINE}, varying from 858.1 seconds to 962.6 seconds (in comparison to 1018.3 and 809.7 seconds for INER and KINE, respectively). As shown in Fig. 5, mean RMSE values vary from 0.12cm to 2.91cm for

287 river water depths and from 0.10$m^3.s^{-1}$ to 5.30$m^3.s^{-1}$ for streamflows, demonstrating a significant
288 improvement in accuracy when compared to KINE.

289 Fig. 6 shows the Amazon River water elevation profile, from its headwater to the outlet,
290 simulated with INER, and errors using KINE and HYBR composed of four flow type maps
291 ($|\Delta rmse|$ thresholds at 1cm, 5cm, 10cm and 20cm). Errors use the INER run as the reference.
292 Profiles are averaged for two seasons: austral fall (April to June, or AMJ), and spring (October to
293 December, or OND). The selected periods respectively coincide with the high (or humid season)
294 and low (dry season) water discharge periods at the outlet. RMSE values for KINE are 4.94m for
295 AMJ and OND, respectively. High inaccuracy is observed in flat central and lower parts of the
296 river, where both the pressure force and inertia are more predominant. In the steep upper part of
297 the river, gravity and friction forces mainly control flow dynamics, hence KINE results in much
298 lower errors. It is worth noting the backwater effect in the lower part of the river in terms of
299 absolute errors. During the dry season, higher water elevations due to the ocean's backwater
300 effect are represented with INER. On the other hand, KINE neglects this effect, resulting in
301 lower water elevations represented by the negative errors, as shown in the figure.

302 Amazon River water elevations simulated by HYBR show significantly lower errors when
303 compared to KINE. RMSE values vary from 4.3cm ($|\Delta rmse| \leq 1cm$) to 6.5cm ($|\Delta rmse| \leq$
304 $20cm$) for AMJ, and from 2.1cm to 3.4cm during the OND period. It is observed that errors
305 occur in the upstream region, where the kinematic wave equation is used. That error is not
306 noticeable in KINE due to the much larger scale used to show its results. There is also a nominal
307 error along the central and lower parts of the river (slightly positive and negative for AMS and
308 OND, respectively), explained by the error propagation from the mainstream headwaters and
309 other tributaries.

310 **4.2. Evaluation against ground and satellite observations**

311 According to Fig. 7, NS values are usually higher in the main rivers and deteriorate near
312 headwaters. This is mostly caused by inaccuracies in both the meteorological forcings and LSM
313 transfers to the river routing scheme, as previously discussed in Getirana et al. (2014b).
314 Comparisons between daily streamflow simulations and observations at 144 gauges show a slight
315 improvement of 0.01 in the mean NS in the realization using INER. However, differences are
316 variable across the basin. At Óbidos, the station draining most of the Amazon basin, located
317 about 800 km upstream from the river mouth, NS values using KINE, INER and HYBR are 0.90,
318 0.91 and 0.91, respectively. In general, both INER and HYBR performed better in the
319 mainstream, and lower parts of Tapajos, Madeira and Purus Rivers. Streamflows derived from
320 HYBR do not show any significant change compared to INER. Such a small average difference
321 of NS is mostly due to the fact that daily time series of streamflow observations are only
322 available where backwater effects are minor or nonexistent. This is explained by the fact that
323 such a variable is derived from rating curve relations where the actual observable variable is
324 river water depth, and that rating curves are only efficiently applicable in steady flow regimes
325 (Fenton et al., 2001).

326 Unlike streamflow observations, radar altimetry enables evaluation of surface water dynamics at
327 any location where satellite tracks intersect water bodies. The 396 radar altimetry stations cover
328 most of the Amazon River and main tributaries, providing us with a detailed picture of how the
329 different methods compare against each other in terms of simulated river water depths. NSA
330 coefficients for river water depths are significantly improved throughout the basin when INER is
331 used compared to KINE (see Fig. 8). The average improvement in NSA is 0.37, with differences
332 mostly present near outlets and confluences, as expected. HYBR, with 64% represented as

kinematic wave equation, results in similar performance coefficients to INER, with a differential NSA of 0.37. This reaffirms the efficiency of a hybrid model in reducing computational costs and keeping relatively high metrics in terms of both streamflows and river water depths.

It is also observed that some locations resulted in efficiency deterioration (negative differential NS and NSA) for both INER and HYBR when compared to KINE. Plausible explanations for such deterioration could be errors in meteorological forcings, limited representations of physical processes in LSMs that are transferred to the river routing scheme. This error transfer may result in random improvements when combined with river routing scheme errors (i.e. errors in the DEM and river geometry parameters). Errors are also explained by both numeric limitations in HyMAP and inaccuracy in the observed data.

Fig. 9 shows bias-corrected daily water elevation time series at the six radar altimetry stations indicated in Fig. 1. Bias values are listed in Table 2 for each location and experiment. Stations were intentionally selected near outlets and confluences in order to expose the improvements obtained using INER. Selected stations are located in the (1) Amazon, (2) Xingu, (3) Tapajos, (4) Madeira, and (5) Negro Rivers and (6) the Solimões near its confluence with the Negro River.

Improvements obtained with both INER and HYBR are clearly noticed at all selected radar altimetry stations. In particular, at station 1, located near the Amazon River outlet, where river flow is highly impacted by the ocean level, both resulted in smoothed water level changes, agreeing with satellite observations. On the other hand, KINE fails in properly simulating water level amplitudes. NSA coefficients are 0.91 for the first two experiments, and -6.50 for KINE. Similar behaviors are noticed at other stations, where INER and HYBR resulted in attenuated amplitudes relative to observations. At station 5, both experiments show improvements in the

peak amplitude and timing, when compared to KINE, resulting in an NSA increase from 0.11 to 0.73. Although improvements are clear, it is noticeable that INER still fails in representing observed amplitudes at some locations. This is particularly noticeable at stations 2, 3 and 5 and could be explained by limitations in the river geometry parameterization, such as inaccurate river width and slope estimates.

5. Summary

In the past decades, the kinematic wave equation has been widely preferred in large-scale river routing schemes for its easy implementation and reduced computational costs. The development of more sophisticated river flow modeling methods, such as the local inertia formulation, has allowed the scientific community to more accurately represent surface water dynamics. Global applications of such new formulations are feasible, but increased computational costs limit the spatial and temporal resolutions. This study evaluates the latter method compared to the kinematic wave equation in terms of precision and computational costs. It also proposes a hybrid model composed of both formulations, where costs can be reduced, maintaining a high accuracy. The spatial distribution of methods in the hybrid model is determined as a function of differential water level RMSE values between INER and KINE runs at 60s time step, based on the principle that river dynamics can be numerically represented by the Saint-Venant equation in a satisfactory way at different levels of complexity determined by dominant flow characteristics (Moussa and Bocquillon, 1996). The evaluation was performed over the Amazon basin in terms of streamflow and water levels and was composed of two steps: (1) accuracy and cost evaluation through synthetic experiments and (2) comparison against in situ and satellite observations. Synthetic experiments considered INER at dt=60s as the reference, and comparisons against observations used 15-minute time step runs.

KINE runs result in large RMSE values along the Amazon River and main tributaries, in particular near the basin's outlet, but these simulations are at least 25% cheaper than the local inertia formulation. INER is numerically stable at time steps lower than 20 minutes. At that time step, a more restrictive CFL condition imposed by the floodplain dynamics limits HyMAP run numerical stability. This is confirmed with the additional adaptive time step run using the CFL condition. On the other hand, KINE shows low model sensitivity to longer time steps, as expected, allowing *dt* as large as three hours with nominal impacts on accuracy. Accuracy was significantly improved with HYBR when compared to KINE, in cases where the local inertia formulation is used in about one third of the basin, with nominal computational cost increase.

Comparisons against in situ and satellite observations show a small overall improvement in simulated streamflows when either INER or HYBR are used, but a significant improvement in water level along main river and tributaries. A possible explanation for such differences in performances is the limited availability of streamflow observations in locations where backwater effects are dominant.

Overall, there is a tradeoff between KINE and INER, and users should choose between accuracy (particularly in locations with predominately diffusive hydraulic processes, such as flat areas) and computational cost. However, combining both the kinematic wave and the local inertia formulations based on flow type maps may result in an optimal compromise between efficiency and computational costs. It is worth noting that the computational cost for runs shown in Table 1 are generally low due to the domain size, spatial resolution and timespan. In particular, costs increase exponentially with increasing spatial resolutions. Long-timespan high-resolution global runs would require a much higher computer power and the additional computational cost could be a critical factor in determining which method to be used. Finally, considering that using the

kinematic wave equation with longer time steps can minimize computational costs preserving numerical stability, future developments could focus on more cost-efficient hybrid models, where spatially distributed time steps would be based on flow types.

Acknowledgements

The study benefited from data made available by the Brazilian Water Agency (Agência Nacional de Aguas: ANA). Radar altimetry data were acquired through the Hydroweb database (http://www.legos.obs-mip.fr/soa/hydrologie/hydroweb/). Surface runoff and baseflow used to force HyMAP are available under request by contacting Augusto Getirana.

References

Arora, V.K., Chiew, F. H. S., Grayson, R. B., 1999: A river flow routing scheme for general circulation models. J. Geophys. Res., 104 (D12), 14 347–14 357.

Bates, P.D., De Roo, A.P.J., 2000. A simple raster-based model for flood inundation simulation. Journal of Hydrology 236 (1–2), 54–77.

Bates, P. D., M. S. Horritt, and T. J. Fewtrell (2010), A simple inertial formulation of the shallow water equations for efficient two-dimensional flood inundation modeling, J. Hydrol., 387, 33–45, doi:10.1016/j.jhydrol.2010.03.027.

Biemans, H., Haddeland, I., Kabat, P., Ludwig, F., Hutjes, R., Heinke, J., von Bloh,W., and Gerten, D. (2011). Impact of reservoirs on river discharge and irrigation water supply during the 20th century. Water Resour. Res., 47(3) :W03509.

Clark, E.A., Sheffield, J., van Vliet, M.T., Nijssen, B. and Lettenmaier, D.P., 2015. Continental

421 runoff into the oceans (1950–2008). Journal of Hydrometeorology, 16(4), pp.1502-1520.

422 Collischonn, W., Allasia, D. G., Silva, B. C., and Tucci, C. E. M.: The MGB-IPH model for
423 large-scale rainfall-runoff modeling, Hydrolog. Sci. J., 52, 878–895, 2007.

424 Cretaux, J. F., Jelinski, W., Calmant, S., Kouraev, A., Vuglinski, V., Berge-Nguyen, M.,
425 Gennero, M.-C., Nino, F., Abarca Del Rio, R., Cazenave, A., and Maisongrande, P.: SOLS:
426 A lake database to monitor in the Near Real Time water level and storage variations from
427 remote sensing data, Adv. Space Res., 47, 1497–1507, 2011.

428 Cunge, J. A., F. M. Holly, and A. Verney (1980), Practical Aspects of Computational River
429 Hydraulics, Pitman Adv. Publ. Program, London.

430 Da Silva, J.S., Calmant, S., Seyler, F., Rotunno Filho, O.C., Cochonneau, G., Mansur, W.J.,
431 2011. Water levels in the Amazon basin derived from the ERS 2 and ENVISAT radar
432 altimetry missions. Remote Sensing of Environment, 114, 2160–2181.

433 David, C.H., Maidment, D.R., Niu, G.Y., Yang, Z.L., Habets, F., Eijkhout, V., 2011. River
434 network routing on the NHDPlus dataset, Journal of Hydrometeorology, 12(5), 913-934.
435 DOI: 10.1175/2011JHM1345.1

436 de Almeida, G. A. M., P. D. Bates, M. Souvignet, and J. E. Freer (2012), Improving the stability
437 of a simple formulation of the shallow water equations for 2D flood modelling, Water
438 Resour. Res., 48, W05528, doi:10.1029/2011WR011570.

439 Decharme, B., R. Alkama, F. Papa, S. Faroux, H. Douville, and C. Prigent, 2012: Global off-line
440 evaluation of the ISBA-TRIP flood model. Climate Dyn., 38, 1389–1412,

441 doi:10.1007/s00382-011-1054-9.

442 Döll, P., Fiedler, K., Zhang, J., 2009. Global-scale analysis of river flow alterations due to water
443 withdrawals and reservoirs. Hydrol. Earth Syst. Sci., 13, 2413–2432.

444 Ek, M., K. Mitchell, L. Yin, P. Rogers, P. Grunmann, V. Koren, G. Gayno, and J. Tarpley, 2003:
445 Implementation of Noah landsurface model advances in the NCEP operational Mesoscale Eta
446 model. J. Geophys. Res., 108, 8851, doi:10.1029/2002JD003296.

447 Fenton, J. D., 2001. Rating Curves: Part 1 – Correction for Surface Slope. The Institution of
448 Engineers, Australia, Conference on Hydraulics in Civil Engineering, 28–30 November
449 2001, Hobart, 309–317.

450 Getirana, A. Boone, D. Yamazaki, B. Decharme, F. Papa, and N. Mognard, 2012: The
451 Hydrological Modeling and Analysis Platform (HyMAP): Evaluation in the Amazon basin. J.
452 Hydrometeor., 13, 1641–1665, doi:10.1175/JHM-D-12-021.1.

453 Getirana, A., McNAlly, A., Roningen, J., Zaitchik, B., Arsenault, K., Jung, H.C., Peters-Lidard,
454 C., 2015. Forecasting Water Availability in Data Sparse and Heavily Managed Catchments in
455 Africa and the Middle East. Gewex News, 27(4), 8-11.

456 Getirana, A.C.V., Boone, A., Peugeot, C., 2014a. Evaluating LSM-based water budgets over a
457 West African basin assisted with a river routing scheme. Journal of Hydrometeorology. DOI:
458 10.1175/JHM-D-14-0012.1

459 Getirana, A., Boone, A., Peugeot, C., 2017. Streamflows over a West African basin from the
460 ALMIP-2 model ensemble. Journal of Hydrometeorology. DOI:

461 http://dx.doi.org/10.1175/JHM-D-16-0233.1.

462 Getirana, A.C.V., Boone, A., Yamazaki, D., N. Mognard, 2013: Automatic parameterization of a
463 flow routing scheme driven by radar altimetry data: Evaluation in the Amazon basin. Water
464 Resour. Res., 49, 614–629, doi:10.1002/wrcr.20077.

465 Getirana, A.C.V., Dutra, E., Guimberteau, M., Kam, J., Li, H., Decharme, B., Zhang, Z.,
466 Ducharne, A., Boone, A., Balsamo, G., Rodell, M., Toure, A.M., Xue, Y., Drapeau, G.,
467 Arsenault, K., Kumar, S.V., Leung, L.R., Peters-Lidard, C., Ronchail, J., Sheffield, J., 2014b.
468 Water balance in the Amazon basin from a land surface model ensemble. Journal of
469 Hydrometeorology. DOI: 10.1175/JHM-D-14-0068.1

470 Getirana, A.C.V., Kumar, S., Peters-Lidard, C., Arsenault, K., 2014c. Water budget in the
471 Amazon basin and impacts on flood modeling, IAHS Publ. 363, 407-412.

472 Getirana, A.C.V., Paiva, R.C.D., 2013. Mapping large scale river flow hydraulics in the Amazon
473 basin. Water Resources Research, 49(5), 2437–2445. DOI: 10.1002/wrcr.20212.

474 Guimberteau, M., and Coauthors, 2012: Discharge simulation in the sub-basins of the Amazon
475 using ORCHIDEE forced by new datasets. Hydrol. Earth Syst. Sci., 16, 911–935,
476 doi:10.5194/hess-16-911-2012.

477 Haddeland, I., Lettenmaier, D.P., Skaugen, T., 2006. Effects of irrigation on the water and
478 energy balances of the Colorado and Mekong river basins, Journal of Hydrology, 324(1-4),
479 210–223.

480 Hanasaki, N., S. Kanae and T. Oki (2006). A reservoir operation scheme for global river routing

models, Journal of Hydrology, 327, 22– 41.

Kirpich, Z. P., 1940: Time of concentration of small agricultural watersheds. Civ. Eng., 10, 362.

Kumar, S.V., Peters-Lidard, C.D., Arsenault, K., Getirana, A.C.V., Mocko, D., Liu, Y., 2015. Quantifying the added value of snow cover area observations in passive microwave snow depth data assimilation. Geophysical Research Letters. DOI: 10.1175/JHM-D-15-0021.1.

Kumar, S.V. et al., 2006. Land information system: An interoperable framework for high resolution land surface modeling. Environmental Modelling & Software 21, 1402-1415. doi:10.1016/j.envsoft.2005.07.004

Kumar, S.V., Zaitchik, B.F., Peters-Lidard, C.D., Rodell, M., Reichle, R., Jasinski, M., Mocko, D., Getirana, A., Cosh, M., Hain, C.R., Anderson, M., Arsenault, K.R., Xia, Y., Ek, M., 2016. Assimilation of gridded GRACE terrestrial water storage estimates in the North American Land Data Assimilation System. Journal of Hydrometeorology, 17, 1951-1972. DOI: 10.1175/JHM-D-15-0157.1 .

Li, H., Leung, L.R., Getirana, A.C.V., Huang, M., Wu, H., Xu, Y., Guo, J., Voisin, N., 2015. Evaluating Global Streamflow Simulations by a Physically-based Routing Model Coupled with the Community Land Model. Journal of Hydrometeorology. DOI: 10.1175/JHM-D-14-0079.1.

Lohmann, D., Nolte-Holube, R., Raschke, E., 1996. A large-scale horizontal routing model to be coupled to land surface parametrization schemes. Tellus Ser. A: Dyn. Meteorol. Oceanogr. 48 (5), 708–721.

501 Luo, X., Li, H., Leung, L.R., Tesfa, T.K., Getirana, A., Papa, F., Hess, L.L., 2017. Modeling
502 surface water dynamics in the Amazon Basin using MOSART-Inundation-v1.0: Impacts of
503 geomorphological parameters and river flow representation. Geoscientific Model
504 Development, 10, 1233–1259. DOI: 10.5194/gmd-10-1233-2017

505 Masson, V., Champeaux, J.-L., Chauvin, C., Meriguet, C., Lacaze, R., 2003. A global database
506 of land surface parameters at 1-km resolution in meteorological and climate models. J.
507 Climate, 16, 1261–1282.

508 Miller, J., G. Russell, and G. Caliri, 1994: Continental scale river flow in climate models. J.
509 Climate, 7, 914–928.

510 Moussa, R., and C. Bocquillon (1996), Criteria for the choice of flood routing methods in natural
511 channels, J. Hydrol., 186, 1–30.

512 Oki, T., and Y. C. Sud, 1998: Design of total runoff integrating pathways (TRIP)—A global
513 river channel network. Earth Interact., 2, doi: 10.1175/1087-
514 3562(1998)002,0001:DOTRIP.2.3.CO;2.

515 Paiva, R.C.D., Collischonn, W., Buarque, D. C., 2013: Validation of a full hydrodynamic model
516 for large-scale hydrologic modelling in the Amazon. Hydrol. Processes, 27, 333–346,
517 doi:10.1002/hyp.8425.

518 Paz, A.R., Collischonn, W., Tucci, C.E.M., Padovani, C.R., 2011. Large-scale modelling of
519 channel flow and floodplain inundation dynamics and its application to the Pantanal (Brazil).
520 Hydrol. Process. 25, 1498–1516. DOI: 10.1002/hyp.7926

521 Reggiani, P., Todini, E., Meißner, D., 2014. Analytical solution of a kinematic wave
522 approximation for channel routing. Hydrology Research, 45(1), 43-57; DOI:
523 10.2166/nh.2013.157

524 Sheffield, J., G. Goteti, and E. F. Wood, 2006: Development of a 50-year high-resolution global
525 dataset of meteorological forcings for land surface modeling. J. Climate, 19, 3088–3111,
526 doi:10.1175/JCLI3790.1.

527 Vorosmarty, C. J., B. Moore III, A. L. Grace, and M. P. Gildea, 1989: Continental scale models
528 of water balance and fluvial transport: An application to South America. Global Biogeochem.
529 Cycles, 3, 241–265, doi:10.1029/GB003i003p00241.

530 Yamazaki, D., G. A. M. de Almeida, and P. D. Bates (2013), Improving computational
531 efficiency in global river models by implementing the local inertial flow equation and a
532 vector-based river network map, Water Resour. Res., 49, 7221–7235,
533 doi:10.1002/wrcr.20552.

534 Yamazaki, D., S. Kanae, H. Kim, and T. Oki, 2011: A physically based description of floodplain
535 inundation dynamics in a global river routing model. Water Resour. Res., 47, W04501,
536 doi:10.1029/2010WR009726.

537

538 Table 1. Synthetic experimental design overview. Computational costs are for two years of
539 simulation and RMSE values are averages for the whole basin, computed relative to INER
540 outputs at dt=60s.

Equation	Time step [s]	Computational cost [s]	Mean RMSE for water level [cm]	Mean RMSE for streamflow [$m^3.s^{-1}$]
Local inertia	60	1018.3	0	0
Local inertia	120	506.0	0.01	0.22
Local inertia	300	205.7	0.03	0.28
Local inertia	600	102.7	0.06	0.41
Local inertia	900	68.7	0.09	0.55
Local inertia	1200	51.3	1.42	26.31
Kinematic wave	60	809.7	19.22	52.27
Kinematic wave	120	412.1	19.22	52.30
Kinematic wave	300	163.3	19.23	52.28
Kinematic wave	600	82.4	19.23	52.26
Kinematic wave	900	55.1	19.24	52.25
Kinematic wave	1200	41.0	19.25	52.24
Kinematic wave	1800	27.2	19.27	52.23
Kinematic wave	3600	13.7	19.34	52.24
Kinematic wave	7200	6.8	19.57	52.37
Kinematic wave	10800	4.6	19.93	52.97
Hybrid ($\lvert\Delta rmse\rvert \leq 1cm$)	60	962.6	0.12	0.10
Hybrid ($\lvert\Delta rmse\rvert \leq 5cm$)	60	902.9	0.84	1.12
Hybrid ($\lvert\Delta rmse\rvert \leq 10cm$)	60	883.1	1.64	2.47
Hybrid ($\lvert\Delta rmse\rvert \leq 15cm$)	60	874.5	2.33	3.79
Hybrid ($\lvert\Delta rmse\rvert \leq 20cm$)	60	858.1	2.91	5.30

541

542 Table 2: Bias correction in meters applied to simulated water elevations at each of the six
543 selected locations shown in Figs. 1 and 9. INER and HYBR outputs have the same bias
544 corrections.

Location	KINE	INER/HYBR
1 (Amazon)	9.32	3.61
2 (Xingu)	1.70	1.05
3 (Tapajos)	3.52	2.64
4 (Madeira)	10.35	8.31
5 (Negro)	10.20	6.13
6 (Solimões)	9.05	10.19

545
546
547

548 Fig. 1: Location of radar altimetry and in situ gauges used in the model evaluation. The location
549 of Óbidos (black triangle) and six radar altimetry stations (black circles) mentioned in the
550 discussion are highlighted.

551 Fig.2: Root mean square error (RMSE) spatial distribution derived from kinematic wave
552 equation experiments at variable time steps (dt), from 60 to 10800 seconds, for river water
553 depths (top) and streamflows (bottom).

554 Fig. 3: Root mean square error (RMSE) spatial distribution derived from local inertia
555 formulation experiments at variable time steps (dt), from 120 to 1200 seconds, for river water
556 depths (top) and streamflows (bottom).

557 Fig. 4: Flow type maps within the Amazon basin based on |Δrmse| thresholds. White and black
558 represent areas simulated using the kinematic wave equation and the local inertia formulation,
559 respectively.

560 Fig. 5: Root mean square error (RMSE) spatial distribution derived from hybrid model
561 experiments at dt=60s and variable |Δrmse| thresholds, from 1 to 20 cm, for river water depths
562 (top) and streamflows (bottom).

563 Fig. 6: Average water elevation profile of the Amazon River for Austral Fall (AMJ) and Spring
564 (OND) averages (1999-2000 period) simulated by the local inertia formulation (top), and errors,
565 relative to the local inertia experiment, resulting from the kinematic wave equation (middle) and
566 the hybrid model composed of four flow type maps with |Δrmse| thresholds at 1cm, 5cm, 10cm
567 and 20cm (bottom).

568 Fig. 7: Nash-Sutcliffe (NS) coefficients of daily streamflows at 144 gauges within the Amazon
569 basin: absolute values using the kinematic wave equation (left); and the differences between the
570 kinematic wave and local inertia formulation (center) and the hybrid model (right).

571 Fig. 8: As Fig. 7, but for Nash-Sutcliffe coefficients of river water depth anomalies (NSA) at 396
572 locations within the Amazon basin.

573 Fig. 9: Water elevation derived from Envisat and simulated by HyMAP using the kinematic
574 wave equation (KINE), the local inertia formulation (INER) and the hybrid model (HYBR) at
575 $|\Delta\mathrm{rmse}| \leq 5\mathrm{cm}$. Simulated water elevations are bias-corrected to match the Envisat mean. The
576 locations are shown in Fig. 1.

577

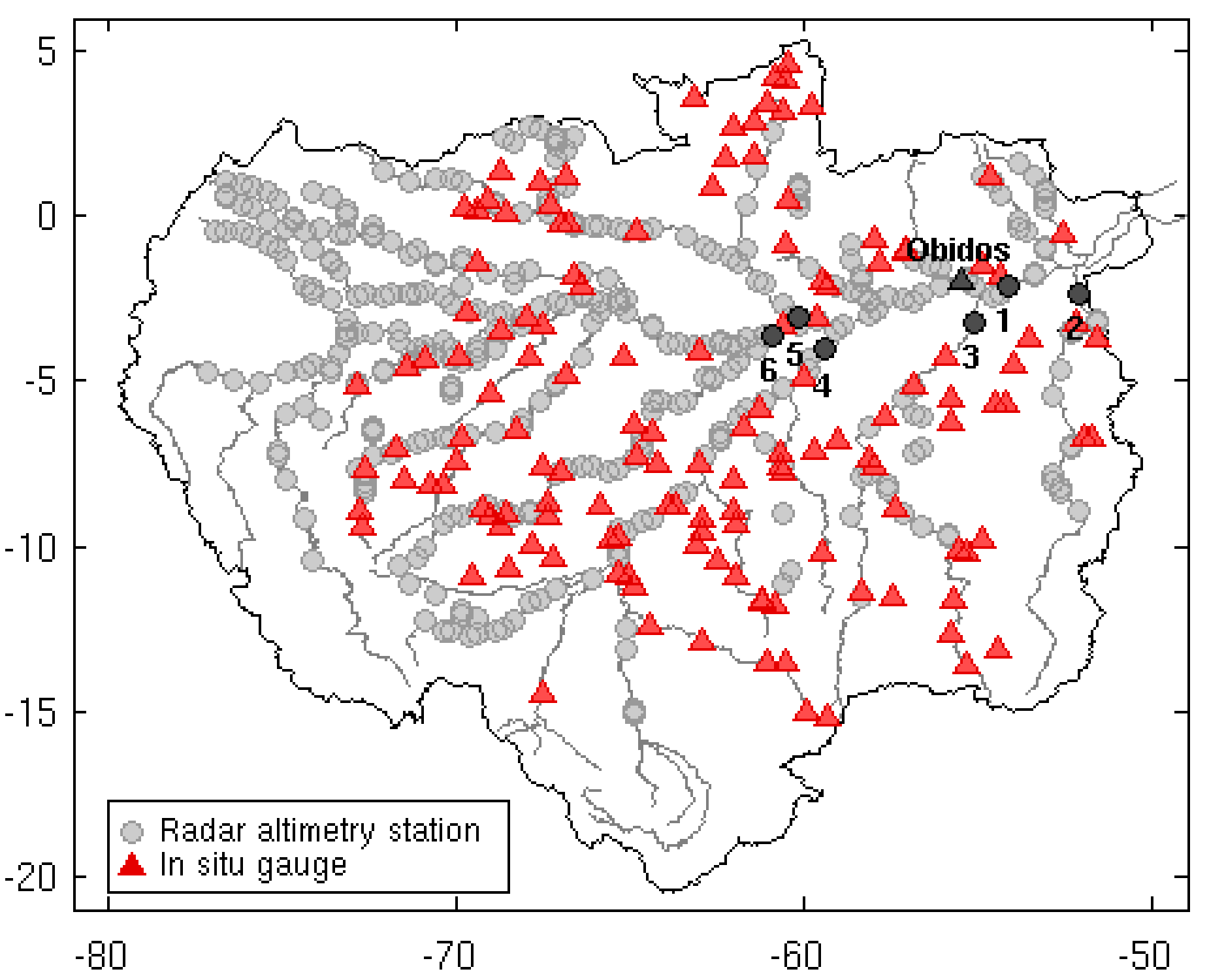
Obidos
1
2
3
4
5
6
Radar altimetry station
In situ gauge
5
0
-5
-10
-15
-20
-80
-70
-60
-50

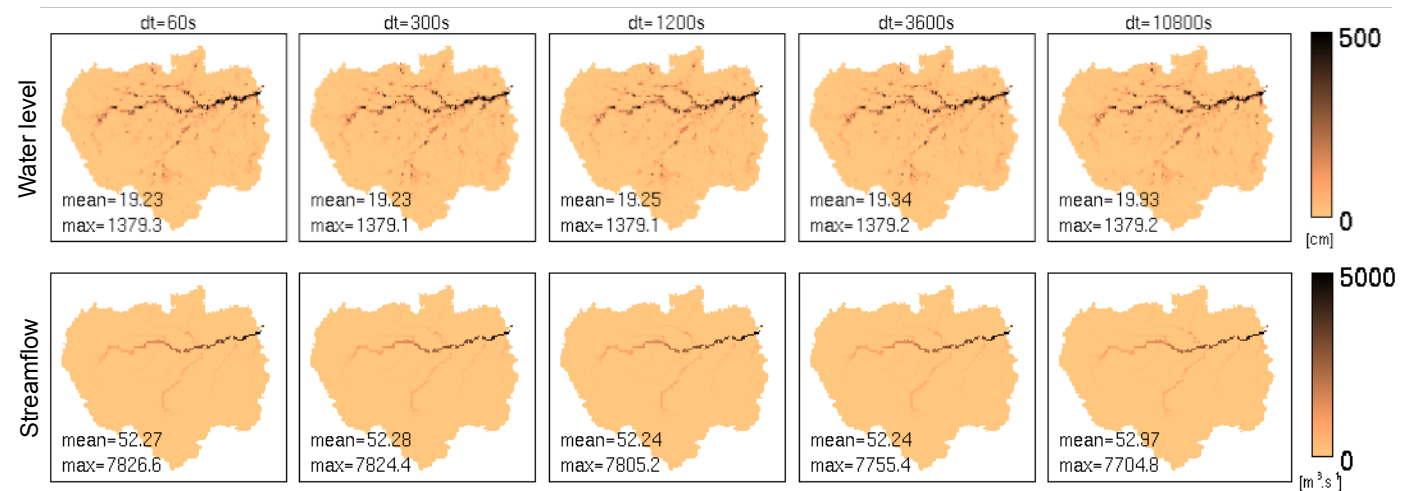
dt=60s
dt=300s
dt=1200s
dt=3600s
dt=10800s
Water level
mean=19.23
max=1379.3
mean=19.23
max=1379.1
mean=19.25
max=1379.1
mean=19.34
max=1379.2
mean=19.93
max=1379.2
500
0
[cm]
Streamflow
mean=52.27
max=7826.6
mean=52.28
max=7824.4
mean=52.24
max=7805.2
mean=52.24
max=7755.4
mean=52.97
max=7704.8
5000
0
[m3.s-1]

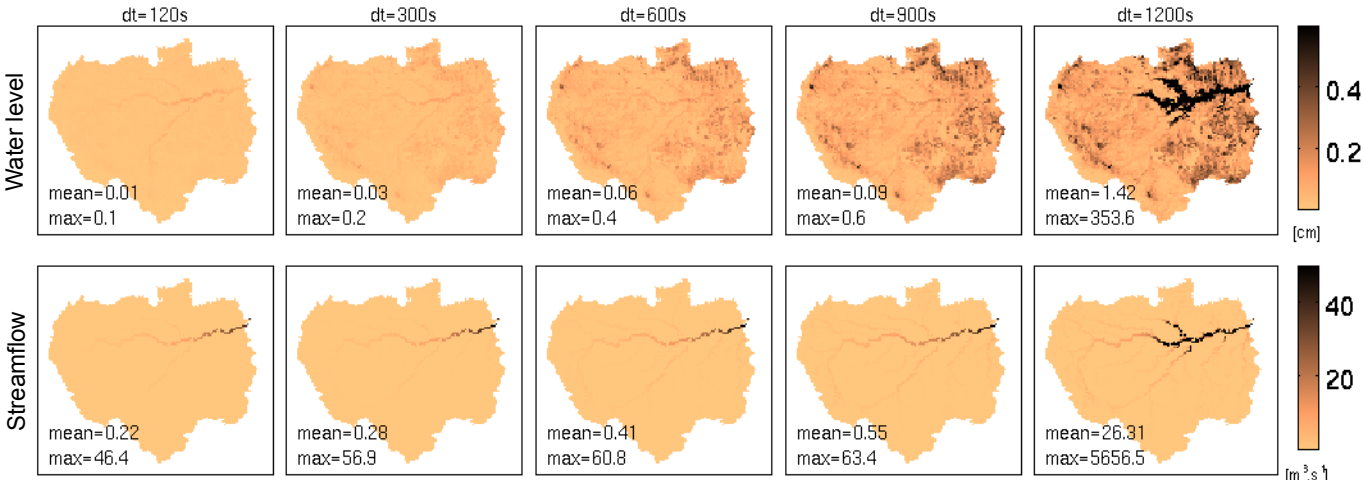
dt=120s
dt=300s
dt=600s
dt=900s
dt=1200s
Water level
mean=0.01
max=0.1
mean=0.03
max=0.2
mean=0.06
max=0.4
mean=0.09
max=0.6
mean=1.42
max=353.6
0.4
0.2
[cm]
Streamflow
mean=0.22
max=46.4
mean=0.28
max=56.9
mean=0.41
max=60.8
mean=0.55
max=63.4
mean=26.31
max=5656.5
40
20
[m 3.s-1]

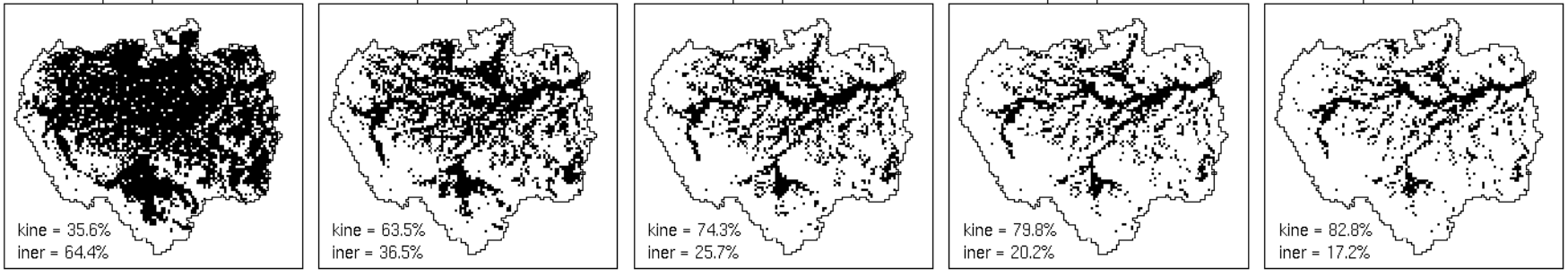
|Δrmse| ≤ 0.01
kine = 35.6%
iner = 64.4%
|Δrmse| ≤ 0.05
kine = 63.5%
iner = 36.5%
|Δrmse| ≤ 0.10
kine = 74.3%
iner = 25.7%
|Δrmse| ≤ 0.15
kine = 79.8%
iner = 20.2%
|Δrmse| ≤ 0.20
kine = 82.8%
iner = 17.2%

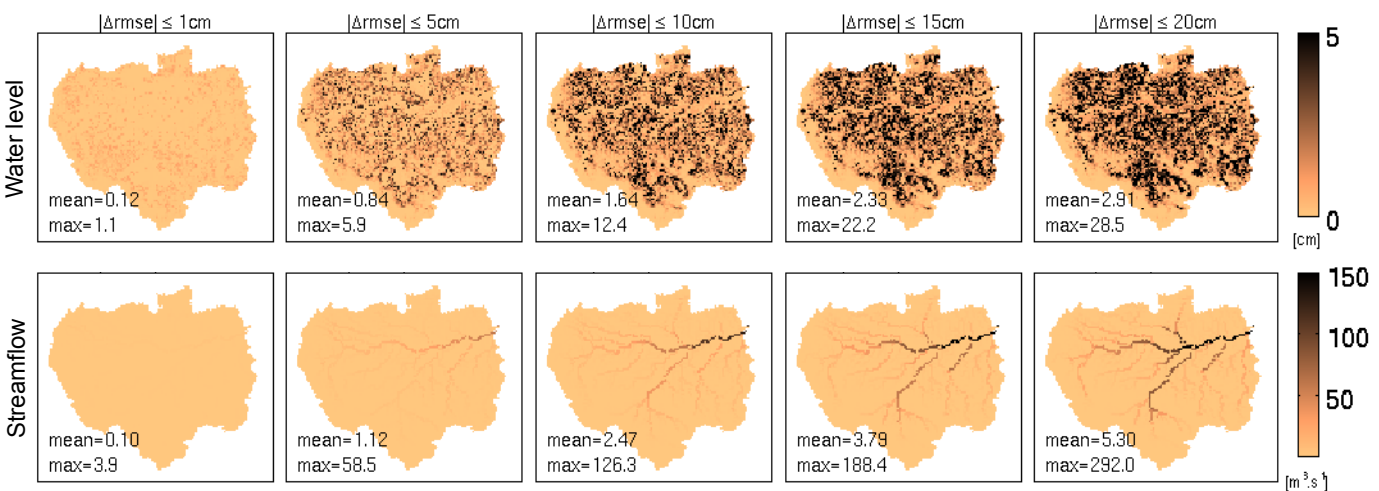
|Δrmse| ≤ 1cm
|Δrmse| ≤ 5cm
|Δrmse| ≤ 10cm
|Δrmse| ≤ 15cm
|Δrmse| ≤ 20cm
Water level
Streamflow
mean=0.12
max=1.1
mean=0.84
max=5.9
mean=1.64
max=12.4
mean=2.33
max=22.2
mean=2.91
max=28.5
5
0
[cm]
mean=0.10
max=3.9
mean=1.12
max=58.5
mean=2.47
max=126.3
mean=3.79
max=188.4
mean=5.30
max=292.0
150
100
50
[m 3.s-1]

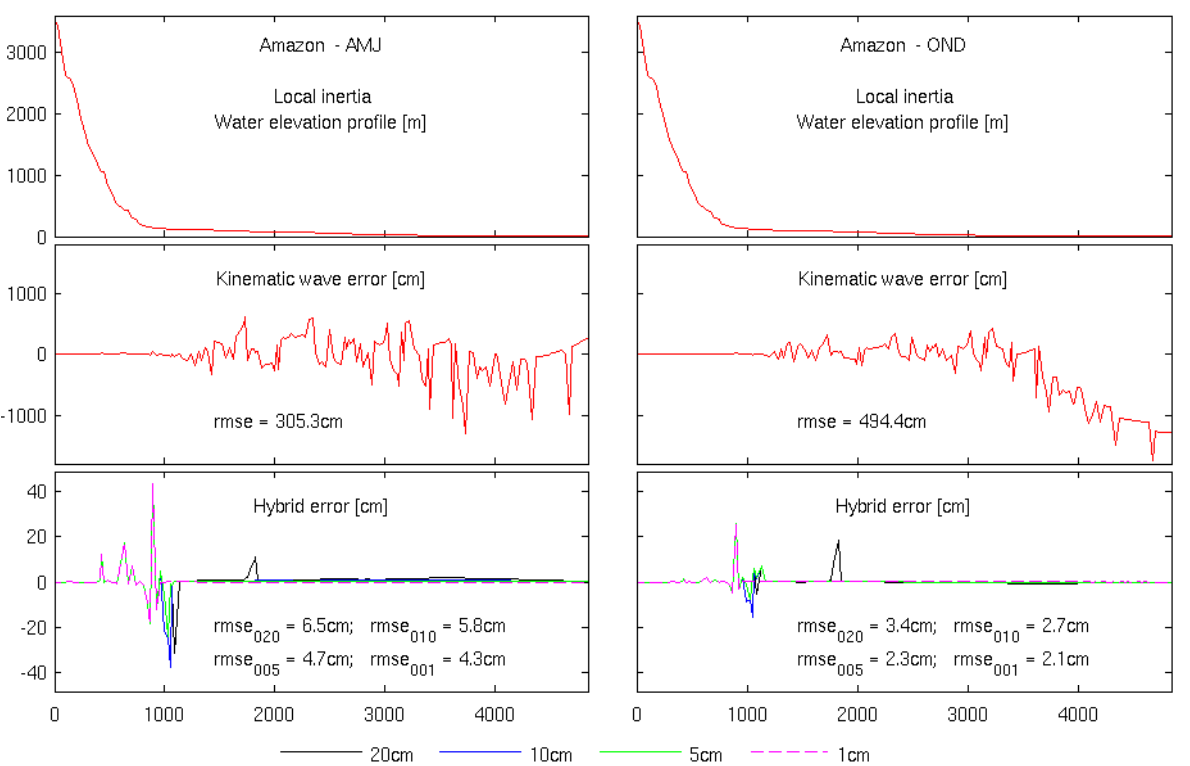
Amazon - AMJ
Local inertia
Water elevation profile [m]
Amazon - OND
Local inertia
Water elevation profile [m]
Kinematic wave error [cm]
rmse = 305.3cm
Kinematic wave error [cm]
rmse = 494.4cm
Hybrid error [cm]
rmse020 = 6.5cm; rmse010 = 5.8cm
rmse005 = 4.7cm; rmse001 = 4.3cm
Hybrid error [cm]
rmse020 = 3.4cm; rmse010 = 2.7cm
rmse005 = 2.3cm; rmse001 = 2.1cm
20cm
10cm
5cm
1cm

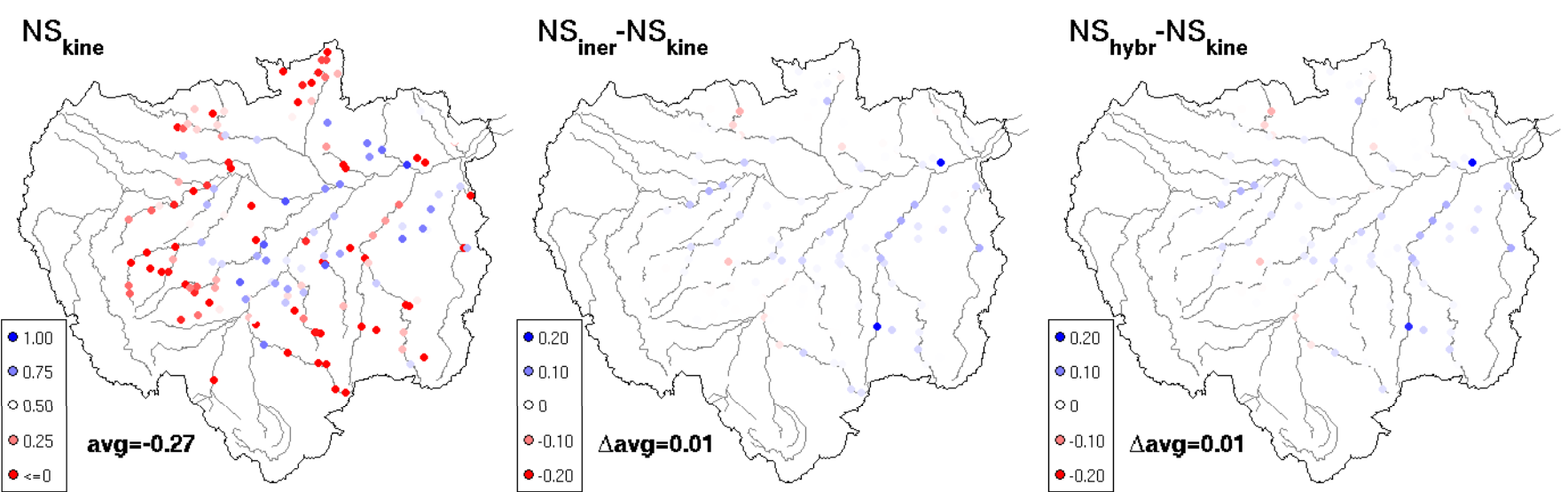
NS kine
1.00
0.75
0.50
0.25
<=0
avg=-0.27
NS iner -NS kine
0.20
0.10
0
-0.10
-0.20
Δavg=0.01
NS hybr -NS kine
0.20
0.10
0
-0.10
-0.20
Δavg=0.01

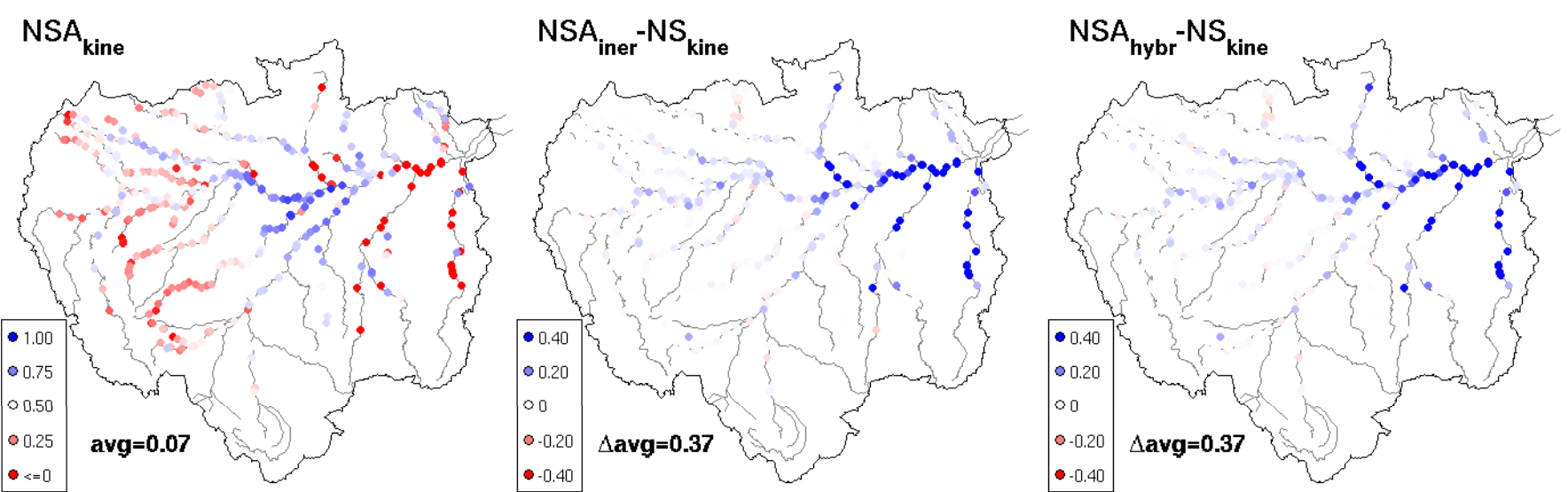
NSA kine
1.00
0.75
0.50
0.25
<=0
avg=0.07
NSA iner -NS kine
0.40
0.20
0
-0.20
-0.40
Δavg=0.37
NSA hybr -NS kine
0.40
0.20
0
-0.20
-0.40
Δavg=0.37

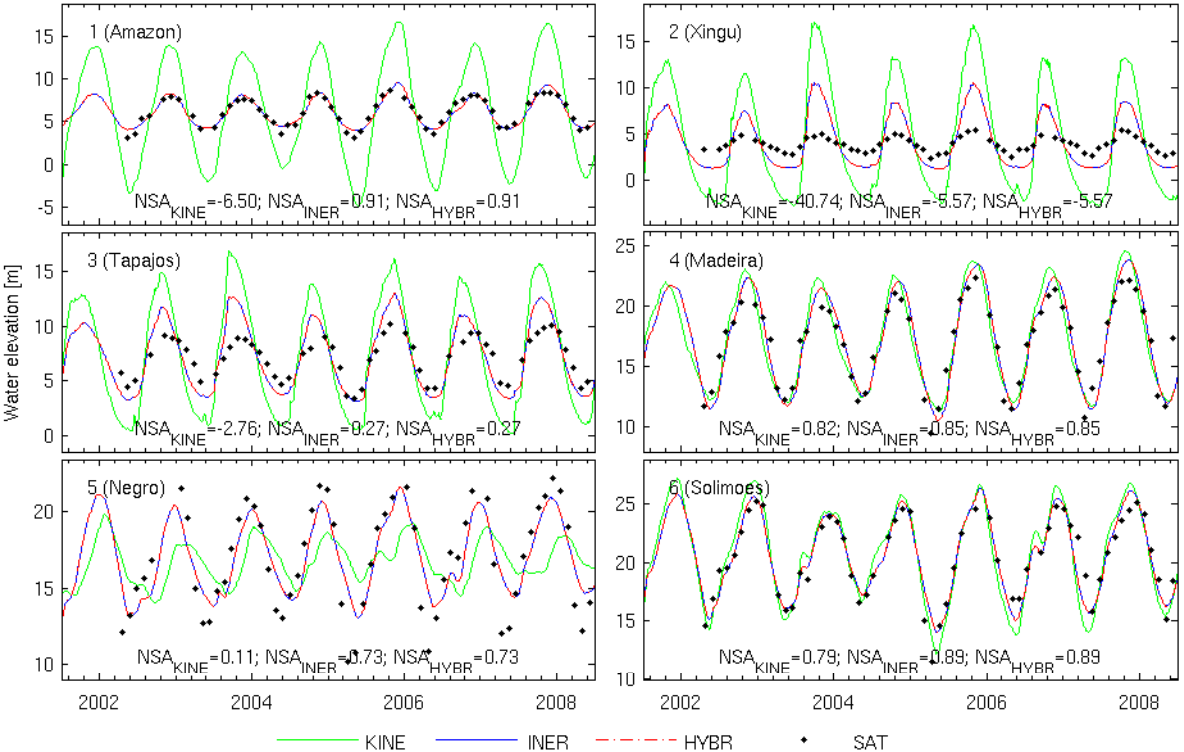
1 (Amazon)
NSA_KINE=-6.50; NSA_INER=0.91; NSA_HYBR=0.91
2 (Xingu)
NSA_KINE=-40.74; NSA_INER=-5.57; NSA_HYBR=-5.57
3 (Tapajos)
NSA_KINE=-2.76; NSA_INER=0.27; NSA_HYBR=0.27
4 (Madeira)
NSA_KINE=0.82; NSA_INER=0.85; NSA_HYBR=0.85
5 (Negro)
NSA_KINE=0.11; NSA_INER=0.73; NSA_HYBR=0.73
6 (Solimoes)
NSA_KINE=0.79; NSA_INER=0.89; NSA_HYBR=0.89
Water elevation [m]
2002
2004
2006
2008
KINE
INER
HYBR
SAT